

# Determination of shower central position in laterally segmented lead-fluoride electromagnetic calorimeters

M. Mazouz<sup>a,\*</sup>, L. Ghedira<sup>a</sup>, E. Voutier<sup>b</sup>

<sup>a</sup>*Faculté des Sciences de Monastir  
Département de Physique  
Monastir 5000, Tunisia*

<sup>b</sup>*Institut de Physique Nucléaire d'Orsay  
IN2P3/CNRS, Université Paris Sud  
15 rue Georges Clémenceau, 91406 Orsay, France*

---

## Abstract

The spatial resolution of laterally segmented electromagnetic calorimeters is studied on the basis of Monte-Carlo simulations worked-out for lead fluoride material. Parametrization of the relative resolution is proposed and optimized in terms of the energy of incoming particles and the elementary size of the calorimeter blocks. A new fit algorithm method is proposed that improves spatial resolution at high energies, and provides guidance for the design optimization of electromagnetic calorimeters.

*Keywords:* calorimeter, electromagnetic shower, impact position, spatial resolution, lead fluoride

---

## 1. Introduction

Electromagnetic calorimeters are fundamental elements of numerous experiments ranging from nuclear to hadronic and high-energy physics. Their main goal is to measure precisely the energy of the detected electrons and photons. The depth of the calorimeters is generally taken to be large enough to avoid energy leaks and to allow a full development of the electromagnetic shower created by the incident particles. In addition to the energy measurement, the impact position of particles, corresponding to the shower central position in case of normal incidence, is usually required in order to provide refined information as particle identification. Indeed, the knowledge of the photon or the electron energy and both the impact and interaction vertex positions allow the determination of the particle four-vector. This is of direct relevance for instance in the experimental determination of the origin of two photon events from the decay of  $\pi^0$ - or  $\eta$ -mesons where the  $2\gamma$ -invariant mass allows identifying the meson

---

\*corresponding author : mazouz@jlab.org

nature. It has been shown in some experiments, that the spatial resolution is of equal importance than the energy resolution for particle identification [1].

The knowledge of the particle impact position requires a laterally segmented calorimeter where the energy is released in a cluster of adjacent blocks. The impact position can then be determined using the energy deposited in each block. Laterally segmented calorimeters such as lead-fluoride ( $\text{PbF}_2$ ) are frequently employed to determine the energy and the position of the showering particle [2, 3, 4]. This high-density material has a short radiation length ( $X_0 = 0.93$  cm) and a small Molière radius ( $r_M = 2.12$  cm) leading to compact detector geometries [5, 6].

Many efforts are still developed for optimizing the performances of such lead-fluoride calorimeters, in particular their energy and spatial resolution [7]. We investigate in this work, on the basis of GEANT4 Monte Carlo simulations [8], the spatial resolution of a  $\text{PbF}_2$  calorimeter for several block sizes and different particle energies. Two approaches are successively considered, discussed, and optimized to obtain a parametrization of the spatial resolution in terms of the block size and the particle energy. Finally, these approaches are compared and the effect of the energy resolution on the spatial resolution is addressed.

## 2. Simulation

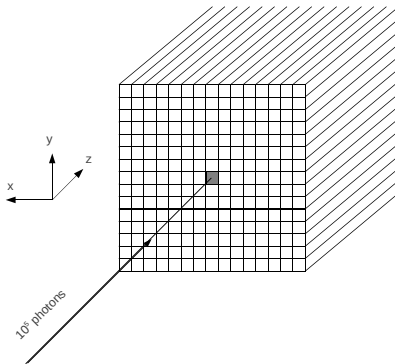


Figure 1: Schematic of the geometry of the simulated calorimeter.

The electromagnetic calorimeter is simulated within the GEANT4 framework following a  $15 \times 15$   $\text{PbF}_2$  block matrix. Each block has a transverse square shape with dimensions  $d \times d$  cm<sup>2</sup> and large enough depth ( $50X_0$ ) along the  $z$ -axis to avoid energy leaks. Different configurations corresponding to 13 different transverse size varying from  $0.3r_M$  to  $5r_M$  are studied. The minimum block size ( $0.3r_M$ ) is consistent with a large enough minimal calorimeter ( $4.5r_M \times 4.5r_M$ ) to contain the electromagnetic shower. For each configuration,

photons of energy  $E$  are sent parallel to the  $z$ -axis and impinge normally on the central region of the calorimeter (Fig. 1). The known impact position  $(x, y)$  of incident particles is distributed uniformly over the area of the central block  $(-d/2, -d/2) < (x, y) < (d/2, d/2)$ . Thirteen photon energies varying from 100 MeV to 20 GeV are generated, leading to a total of 169 configurations. In each case, the response on the calorimeter is studied for  $10^5$  generated initial photons: the event-by-event energy deposit in each individual block is recorded and used to reconstruct the shower central position  $(x_c, y_c)$  as described in the following sections. Focus is put here only on the  $x_c$  coordinate since the  $y_c$  coordinate can be deduced following the same methods.

Two approaches can be used for reconstructing the shower central position  $x_c$ . The first method is based on a numerical formula depending on the  $x_i$ -coordinate of the  $i^{th}$  block center and the energy deposit  $E_i$  in this block. The second method developed in the present work relies on fitting the calorimeter block response with a known profile function where  $x_c$  becomes the free parameter of the fit.

### 3. Formula based method

Various formulas have been proposed to determine the shower central position [9, 10, 11, 12, 13]. The center of gravity method is one of the most common formula

$$x_c = \frac{\sum_i w_i x_i}{\sum_i w_i} , \quad (1)$$

where the sum runs over the number of blocks in the shower cluster and  $w_i$  is a weight factor depending of the energy  $E_i$ . In the simplest case where  $w_i = E_i$ , it has been shown that the obtained  $x_c$  depends on  $x$  in a non-linear way. A term, depending of the size  $d$  of the blocks and the exponential radial falloff of the shower, has to be added to Eq. 1 to correct from the correlation between  $x_c - x$  and  $x$  [9], the so-called *S-curve*. Many other formulas and algorithms have been discussed and compared in reference [11]. For example, the un-shifted estimate of  $x_c$  based on here-after expressions (Eq. 2-3) reduces significantly the non-linear correlation between  $x$  and  $x_c$  and gives a satisfying reconstruction of the shower position

$$x_c = x_m + \frac{\sigma_1}{2} \ln \left( \frac{E_{m+1}}{E_{m-1}} \right) , \quad (2)$$

$$x_c = x_m \pm d \mp \sigma_2 \ln \left( \frac{1}{2} \left[ 1 + \frac{E_m}{E_{m\pm 1}} \right] \right) . \quad (3)$$

In the previous relations  $x_m$  represents the coordinate of the block with a maximal energy deposition and  $\sigma_1$  and  $\sigma_2$  are related to the transverse exponential behavior of the shower [11]. This un-shifted estimate of  $x_c$  uses only the information of two particular blocks: the ones with the largest energy deposition (Eq. 3) and the ones adjacent to the block with maximal energy (Eq. 2). In comparison to the simplest energy weighting case, the logarithmic weighting of

energies in these expressions procures a stronger influence of low energy deposit blocks in the calculation of  $x_c$ . Lately, a simple method based on Eq. 1 has been proposed and is still largely employed nowadays in many experimental analysis. It has been shown that it gives results similar or superior in quality to all those discussed previously and does not need position correction [13]. In this method the energy weight  $w_i$  is given by

$$w_i = \max \left\{ 0; W_0 + \ln \left( \frac{E_i}{E} \right) \right\} \quad (4)$$

where  $W_0$  is a free dimensionless parameter. Consequently, only the blocks having an energy deposition higher than  $Ee^{-W_0}$  are taken into account in the calculation of  $x_c$ . In addition  $W_0$  allows to set the relative weight of the blocks, with a small energy deposition, used in the sum of Eq. 1. Indeed, high  $W_0$  values attribute almost an equal weight to the blocks entering the sum, while small  $W_0$  values favor the highest energy blocks. It exists therefore an optimal  $W_0 \approx 4$  giving the best position reconstruction [13].

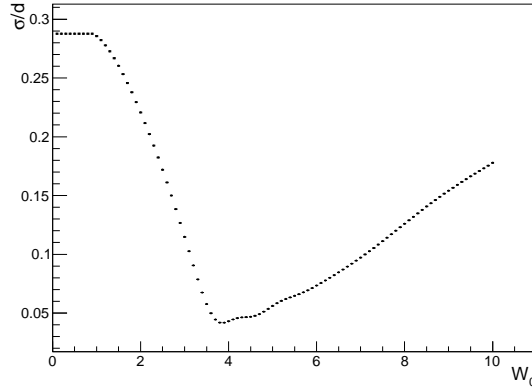


Figure 2: Relative position resolution  $\sigma/d$ , for  $d = r_M$  and  $E = 10$  GeV, as a function of  $W_0$  (statistical uncertainties are smaller than the point size).

Actually the optimal  $W_0$  value, called  $W_0^{for}$  hereafter to indicate the formula method origin of this parameter, depends on the size  $d$  of the blocks as well as the energy  $E$  of the incident particle. Fig. 2 shows a typical behavior of the position resolution  $\sigma$ , defined by the root mean square (RMS) of the  $(x_c - x)$  distribution, as a function of  $W_0$ . The minimal value of  $\sigma$  defines  $W_0^{for}$  whereas the worst resolution obtained for  $W_0 = 0$  or  $W_0 \rightarrow +\infty$  equals  $d/\sqrt{12}$  and corresponds to the RMS of a uniform distribution of width  $d$ . The optimal  $W_0^{for}$  and corresponding position resolution  $\sigma^{for}$  are determined for each geometry and energy configuration previously described (Sec. 2). Fig. 3 shows the energy dependence of  $W_0^{for}$  for different block sizes. At a given size, the energy deposit in the blocks surrounding the central block becomes small and very sensitive to

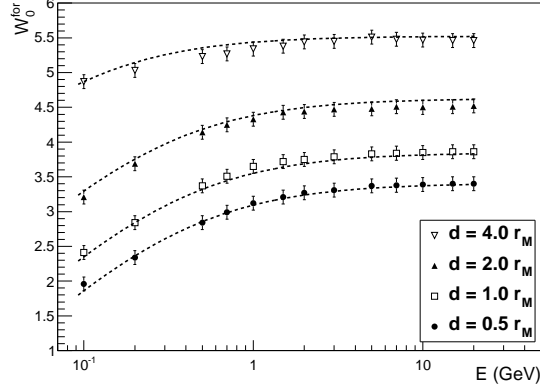


Figure 3: Energy dependence of  $W_0^{for}$ . The block size  $d$  relative to the Molière radius is reported in the legend for each configuration. Dashed lines represent the parametrization of Eq. 5. The 0.1 uncertainty on  $W_0^{for}$  corresponds to the bin size of Fig. 2.

the sampling fluctuations of the shower when the energy  $E$  decreases. Including these blocks in the calculation of  $x_c$  could then degrades the resolution. These blocks are removed by small  $W_0$  values as shown on Fig. 3. At given energy  $E$ ,  $W_0^{for}$  increases as the block size  $d$  becomes larger. Indeed, for large blocks the energy of the shower is essentially deposited in the central block. Having a high threshold with small  $W_0$  excludes the remaining blocks and the  $x_c$  position becomes the central block coordinate with a resolution relative to the block size. An empirical parametrization of  $W_0^{for}$  as function of  $d$  and  $E$  is proposed here following the expression

$$W_0^{for} = \ln \left( \frac{100 E(\text{GeV})}{2.01 e^{-\frac{d}{r_M}} + [4.95 e^{-\frac{d}{r_M}} + 0.307] E(\text{GeV})} \right) \quad (5)$$

where the three numerical constants are determined from a global fit of the 169 configurations. Fig. 3 shows the result of this parametrization for some particular values of  $d$ .

The obtained resolution  $\sigma^{for}$  is represented on Fig. 4 as function of  $E$  for different block sizes.  $\sigma^{for}$  is expected to scale with  $1/\sqrt{E}$  at high energies [14]: the relative energy resolution  $\sigma_i/E_i$  for each block  $i$  is proportional to  $1/\sqrt{E_i}$  and then to  $1/\sqrt{E}$ , assuming the same average shower profile; all the terms in Eq. 1 having then a relative precision proportional to  $1/\sqrt{E}$ ,  $\sigma^{for}$  is also scaling as  $1/\sqrt{E}$ . At low energies ( $E \ll 1$  GeV), this proportionality becomes not valid since the worst resolution one could obtain cannot exceed  $d/\sqrt{12}$ . The  $E$ -dependent  $\sigma^{for}$  graphs for each block size are fitted at high energies with the expression

$$\frac{\sigma^{for}}{d} = \frac{\alpha}{\sqrt{E}} + \beta \quad , \quad (6)$$

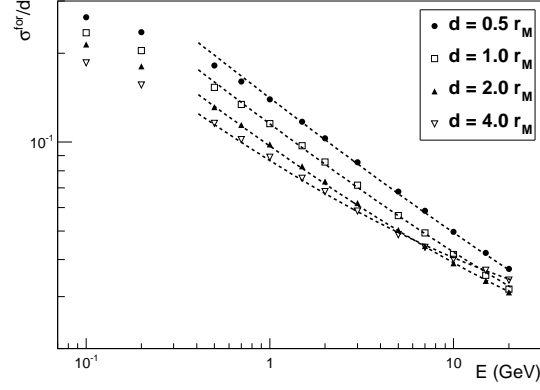


Figure 4: Energy dependence of the relative resolution. Dashed lines represent Eq. 8 parametrization.

where  $\alpha$  and  $\beta$  are the free parameters of the fit. The resulting coefficient  $\alpha$  is represented on Fig. 5 as function of the block size. The  $d$ -dependence of  $\alpha$  can be parametrized as

$$\alpha = a^{for} \left( \frac{d}{r_M} \right)^{b^{for}} \quad (7)$$

where  $a^{for}$  and  $b^{for}$  are two constants relative to the formula method. The

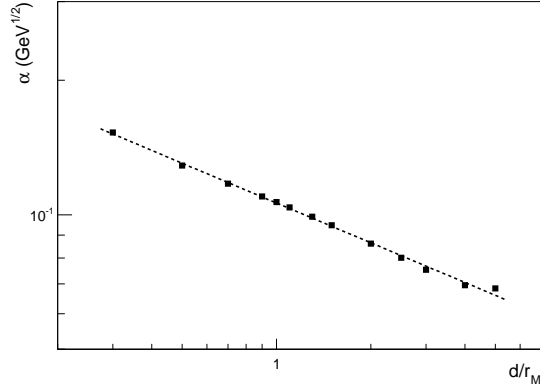


Figure 5: The fitted coefficient  $\alpha$  as a function of  $d$  (in  $r_M$  units).

global fit of the  $\sigma^{for}$  resolution for each configurations leads to the semi-empirical

parametrization of the relative resolution

$$\frac{\sigma^{for}}{d} = \frac{a^{for} \left(\frac{d}{r_M}\right)^{b^{for}}}{\sqrt{E(\text{GeV})}} + c^{for} \left(\frac{d}{r_M}\right) + d^{for} \quad (8)$$

where  $a^{for} = 0.110$ ,  $b^{for} = -0.334$ ,  $c^{for} = 3.55 \times 10^{-3}$  and  $d^{for} = 4.02 \times 10^{-3}$ . The results of this expression are shown in Fig. 4 for some particular block sizes. It is obvious from Eq. 8 that the resolution  $\sigma^{for}$  becomes better at high energies and for small block sizes. However, the  $d$ -dependence of the relative resolution  $\sigma^{for}/d$  at fixed energy is more involved. It is worth noting that Eq. 8 suggests the existence of an optimum block size corresponding to an optimum relative resolution at a given  $E$ , allowing optimizing the calorimeter block size for a given energy measurement range.

#### 4. Fit based method

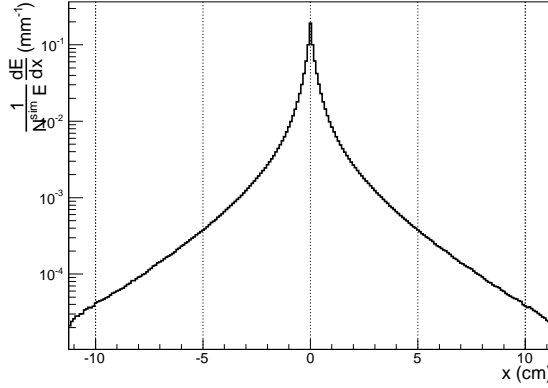


Figure 6: Average shower profile function for  $E=1$  GeV photons.

A second approach for reconstructing the shower central position relies on the knowledge of the lateral profile of the electromagnetic shower. Fig. 6 shows the profile function  $F(x)$  obtained from the simulated response of an infinite lead fluoride calorimeter to  $N_{sim}=10^5$  photons of 1 GeV. This response is represented as function of the distance from the shower center along  $x$ -axis. The energy deposit is here determined per generated photon, as the transverse dimension integral normalized by the initial photon energy

$$F(x) = \frac{1}{N_{sim}} \frac{1}{E} \int_{-\infty}^{+\infty} \frac{d^2 E(x, y)}{dx dy} dy = \frac{1}{N_{sim}} \frac{1}{E} \frac{dE(x)}{dx} \quad (9)$$

where  $dE(x)$  is the energy released by the shower in a vertical column calorimeter centered at  $x$ , having a width  $dx=1$  mm and an infinitely large height. This

profile function turns out to be the same for photons and electrons and no energy dependence is expected according to the definition of the Molière radius.

In Ref. [11], the shower profile was approximated by a single exponent term and a least-squares fit algorithm was developed for extracting the shower position taking into account all of the responding blocks of the calorimeter. It was shown that the results are similar to those obtained with Eq. 2 and Eq. 3 [11], and do not present any significant advantage relatively to the fast and simple method based on Eq. 1-4 [13]. Nevertheless, it is clear from Fig. 6, that the lateral profile of the shower is a more intricate function different from a simple exponent or a combination of two exponent contributions. A more realistic form  $F(x)$  of the profile function is proposed in the present work, deduced from the bin-to-bin linear interpolation of the simulated profile function (Fig. 6).

In the calorimeter described in section 2, the expected energy deposit for a given simulated event in a column  $i$  identified by its central coordinate  $x_i$  writes

$$E_i^{exp} = E \int_{x_i-d/2}^{x_i+d/2} F(x - x_c) dx \quad (10)$$

where  $x_c$  is the unknown shower central position, and  $E$  is the incident particle energy corresponding to the total energy deposit in the calorimeter if we neglect the energy resolution effect. The clear energy deposit in that column for the same event expresses

$$E_i = \sum_j E_{ij} \Theta(E_{ij} - E e^{-W_0}) \quad (11)$$

where  $W_0$  is a dimensionless parameter related to the energy threshold applied on the blocks, and  $\Theta(x)=1$  when  $x > 0$  and 0 otherwise is the Heaviside function. In the previous equation,  $E_{ij}$  represents the energy deposit in the block belonging to column  $i$  and row  $j$ . Fitting for each event, with the MINUIT package [15], the  $E_i$  distribution (Eq. 11) with the expected distribution  $E_i^{exp}$  (Eq. 10) allows to extract the single free parameter of the fit  $x_c$ . Following Eq. 11, this algorithm rejects the blocks with energy deposit smaller than the threshold  $E e^{-W_0}$ .

Fig. 7 shows the influence of  $W_0$  on the obtained resolution  $\sigma$  given by the RMS of the  $(x_c - x)$  distribution for a particular value of  $E$  and  $d$ . As expected, larger the block number contributing to Eq. 11, better the relative resolution. However, the resolution remains constant after a certain  $W_0$  since very small energy deposit blocks do not contribute significantly to  $x_c$  calculation and consequently not change the fit result. The optimum  $W_0$ , denoted  $W_0^{fit}$  here-after, is defined as the value above which the resolution does not improve by more than 1%. No real energy dependence of  $W_0^{fit}$  is observed but logarithmic scaling with the block size is demonstrated on Fig. 8, following the parametrization

$$W_0^{fit} = 1.61 \ln \left( \frac{d}{r_M} \right) + 5.55 \quad . \quad (12)$$



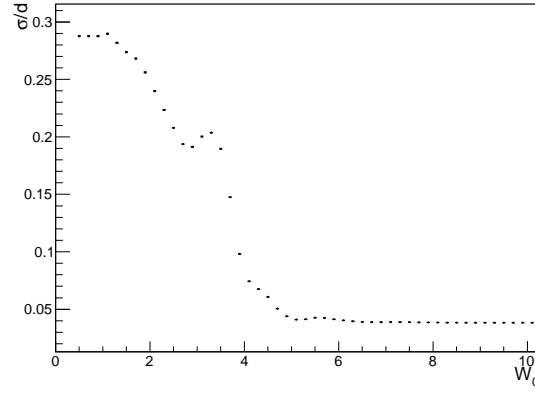


Figure 7:  $W_0$ -dependence of the relative position resolution  $\sigma/d$ , for  $d=r_M$  and  $E=10$  GeV.

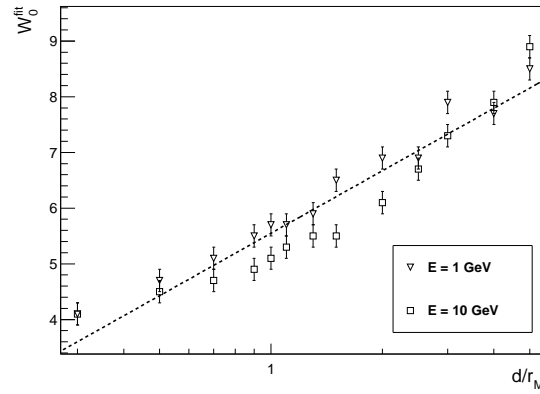


Figure 8: Block size dependence of  $W_0^{fit}$  for two different photon energies; the dashed line corresponds to Eq. 12 parametrization.

For large block size, the shower energy is mainly deposited in one single block so the energy threshold must be reduced to include the surrounding blocks in order to improve the spatial resolution.

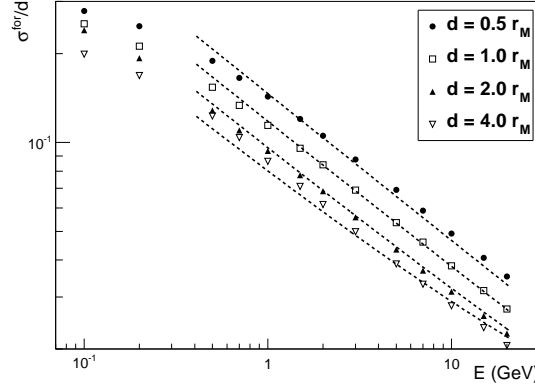


Figure 9: The relative resolution  $\sigma^{fit}/d$  as a function of the shower energy  $E$ . The block size  $d$  is indicated in the legend for each configuration. Dashed lines represent the parametrization of Eq.13.

The relative resolution of the fit method here developed is represented in Fig. 9 as function of the shower energy  $E$  for different block sizes. As for the formula method, the resolution can be parametrized following the expression

$$\frac{\sigma^{fit}}{d} = \frac{a^{fit} \left( \frac{d}{r_M} \right)^{b^{fit}}}{\sqrt{E(\text{GeV})}} + c^{fit} \left( \frac{d}{r_M} \right) + d^{fit} , \quad (13)$$

where  $a^{fit} = 0.121$ ,  $b^{fit} = -0.349$ ,  $c^{fit} = 1.78 \times 10^{-3}$  and  $d^{fit} = 1.89 \times 10^{-3}$ . These four constants are deduced from a global fit of the studied configurations.

The fit algorithm described in this section is obviously more computing time consuming at the data analysis level than the formula based method. Nevertheless, modern computers can easily and efficiently handle this problem: for instance, more than  $10^4$  events per second can be analyzed with a modest 2 GHz processor.

## 5. Discussion

### 5.1. Comparison of the formula and fit methods

The formula and fit methods are compared on Fig. 10 from a typical distribution of the shower central position obtained for a given configuration. In opposition to the fit determination, the formula determination of  $x_c$  does not exhibit the constant behavior expected from the uniform generation of the shower  $x$  origin. This appears as a consequence of the number of blocks taken into

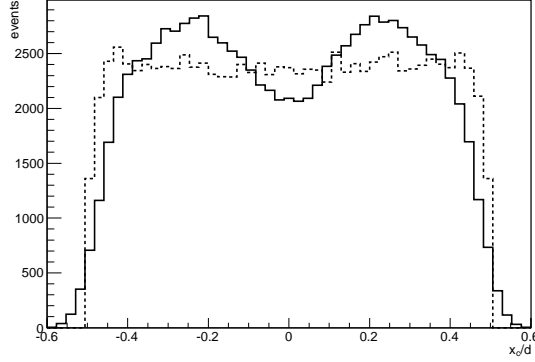


Figure 10: Reconstructed shower position  $x_c$  (in block size units) using the formula method (solid line) and the fit method (dashed line) for  $d = r_M$  and  $E = 5$  GeV.

account in Eq. 1. It was found in this study that the average number of blocks entering Eq. 1 is approximately 4 but could slightly differ depending on the configuration type (for instance, 4.2 in the configuration shown on Fig. 10). Therefore on average, two different block coordinates only are contributing to the determination of  $x_c$  in Eq. 1, which slightly favors the region between the center and the boundaries of the central block. This restriction does not show-up in the fit method where  $W_0^{fit}$  is always larger than  $W_0^{for}$  and allows a larger number of blocks to contribute to the determination of the shower central position.

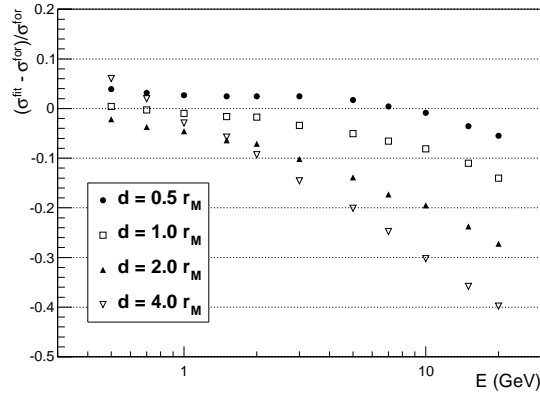


Figure 11: Energy dependence of the relative difference between the formula and fit methods. The block size  $d$  is indicated in the legend for each configuration.

Fig. 11 shows the relative difference between the spatial resolution obtained with the two previously described methods. For small block sizes, the formula

based method tends to be slightly preciser than the fit based method. However, when the block size comes closer or higher than the Molière radius, the fit based method can provide as high as 40% better resolution at high energies. Within the present work, particles with normal incidence only are considered whereas experimentally one can have different incident angles. It has been shown that the position resolution obtained with the formula based method is rather insensitive to this angle for moderate values [13]. For large incidence angles, a simulation optimizable geometrical correction depending on the shower depth must be taken into account since the impact position of the particle is shifted relatively to the shower central position [16]. Similarly, different lateral shower profile functions depending on the incidence angle can be simulated and exported within the fit method to obtain the shower position and the corrected impact position.

### 5.2. Effect of the energy resolution

The resolution of the energy measurement per block originates solely from the shower sampling fluctuations in the current simulation approach. Experimentally, lead-fluoride calorimeters are based on the detection of Čerenkov light and the fluctuations in the number of collected photo-electrons dominates the energy resolution [14]. The generation and tracking of Čerenkov photons is not performed here because of unrealistic computing times and strong sensitivity to exact optical properties of crystal and wrapping surfaces which are known to differ from an experimental device to another. This effect can globally be symbolized by an additional smearing of the energy deposition  $E_i$  in each block  $i$ . This is done by adding to  $E_i$  a random number following a Gaussian distribution centered at zero and having the following width

$$\sigma^s = s \sqrt{E_i} , \quad (14)$$

where  $s$  is a constant related to the global relative energy resolution of the calorimeter. Several  $s$ -values in the range 1%-20% are used in the following to study the effect of the energy resolution on the position resolution. The degradation of the position resolution  $\sigma$  is defined as

$$\sigma^{deg} = \sqrt{\sigma^2(s) - \sigma^2(s=0)} \quad (15)$$

where  $\sigma(s)$  is the position resolution at a given  $s$ -value, and  $\sigma(s=0)$  is the position resolution in absence of energy smearing, both determined for any of the two methods. This study shows that  $\sigma^{deg}$  is proportional to  $s$ .

Fig.12 shows the typical energy dependence of the relative average resolution  $\sigma^{deg}/s/d$  for a particular block size. As expected from Eq. 14, the degradation of the position resolution can be parametrized at high energies

$$\frac{1}{s} \frac{\sigma^{deg}}{d} = \frac{a^{deg}}{\sqrt{E}} \quad (16)$$

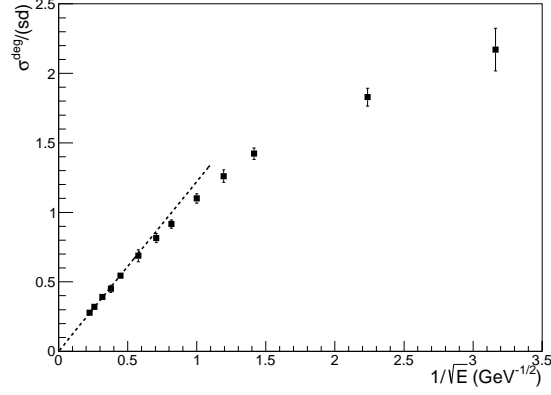


Figure 12:  $\sigma^{deg}/s/d$  as a function of  $1/\sqrt{E}$  for the  $d = r_M$  configuration. The same behavior is observed for other configurations which are omitted sake of clarity.

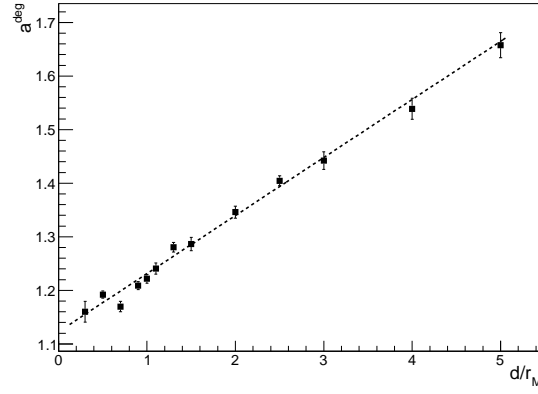


Figure 13: The fitted parameter  $a^{deg}$  (Eq. 16) as a function of  $d/r_M$ . The dashed line corresponds to the relation  $a^{deg}=0.112 \left( \frac{d}{r_M} \right) + 1.12$  and represents the first order polynomial fit of the distribution.

where  $a^{deg}$  is a parameter depending linearly on the block size  $d$  as shown on Fig. 13. Finally the obtained position resolution  $\sigma$  taking into account energy resolution effects can be expressed

$$\frac{\sigma}{d} = \frac{\sigma^{for,fit}}{d} \oplus s \frac{0.112 \left( \frac{d}{r_M} \right) + 1.12}{\sqrt{E(\text{GeV})}} \quad (17)$$

where  $\sigma^{for,fit}$  is either given by Eq. 8 or Eq. 12 according to the chosen method of the position determination.

Experimentally, other effects such as the physics and electronics background, energy calibration, radiation damage... can contribute to the energy resolution and then degrades the position resolution. However, in a well designed experiment these effects are not dominating the position resolution. Finally, the systematic uncertainty coming from the experimental knowledge of the coordinates  $x_i$  of the block centers has to be added quadratically to Eq. 17 to obtain the final position resolution but this contribution can generally be neglected, as connected to the accuracy of the mechanical design and mounting. In Ref. [3], the obtained experimental resolution on the reconstructed position using the center of gravity method is 2 mm, in good agreement with the 1.9 mm predicted by Eq. 17.

## 6. Conclusion

The present work discussed the determination of the shower central position in a laterally segmented electromagnetic calorimeter following the widely used center of gravity method and a new fit method here developed. A semi-empirical parametrization of the relative position resolution as a function of the incident particle energy and the calorimeter block size is proposed and optimized for each case. The fit method is shown to significantly improve the position resolution as compared to the formula method, particularly at high energies and for large block sizes. Finally, energy resolution effects on the position resolution are also discussed and quantified.

Despite the present application to lead-fluoride calorimeters, the results presented here can be exported to several electromagnetic calorimeter materials through their parametrization in terms of the Molière radius. In addition, as far as simulations are concerned, the profile function at the heart of the fit method has energy and material universality features. This global study not only provides useful parametrization for the design optimization of electromagnetic calorimeters in future experiments looking for a good spatial resolution, but procures also a new algorithm to improve position resolution at the data analysis level.

## References

### References

- [1] R.T. Jones et al., Nucl. Instr. and Meth. A 566 (2006) 366.

- [2] M. Mazouz et al., Phys. Rev. Lett. 99 (2007) 242501.
- [3] C. Muñoz Camacho et al., Phys. Rev. Lett. 97 (2006) 262002.
- [4] F.E. Maas et al., Phys. Rev. Lett. 93 (2004) 022002.
- [5] D.F. Anderson et al., Nucl. Instr. and Meth. A290 (1990) 385 .
- [6] <http://pdg.lbl.gov/2011/AtomicNuclearProperties>
- [7] A.T. Fienberg et al., Nucl. Instr. and Meth. A783 (2015) 12.
- [8] R. Brun, et al., GEANT User's Guide, Program Library W5013, CERN.
- [9] G.A. Akopjanov et al., Nucl. Instr. and Meth. 140 (1977) 441.
- [10] V.A. Davydov et al., Nucl. Instr. and Meth. 145 (1977) 267.
- [11] L. Bugge, Nucl. Instr. and Meth. A242 (1986) 228.
- [12] J.J. Gomez et al., Nucl. Instr. and Meth. A262 (1987) 284.
- [13] T.C. Awes et al., Nucl. Instr. and Meth. A311 (1992) 130.
- [14] R. Wigman, International Series of Monographs on Physics, vol. 107, Oxford University Press, Oxford, 2000.
- [15] F. James and M. Roos, Comp. Phys. Comm. 10 (1975) 343.
- [16] A.N. Vasil'ev et al., Instr. and Exp. Tech. 50 (2007) 458.